Available online at www.sciencedirect.com
SCIENCE DIRECT®
Journal of Catalysis 222 (2004) 470–480
JOURNAL OF CATALYSIS
www.elsevier.com/locate/jcat

Effect of sodium addition on the performance of Co–ZnO-based catalysts for hydrogen production from bioethanol

Jordi Llorca,[a] Narcís Homs,[a] Joaquim Sales,[a] José-Luis G. Fierro,[b] and Pilar Ramírez de la Piscina [a,*]

[a] *Departament de Química Inorgànica, Universitat de Barcelona, C/Martí i Franquès 1-11, 08028 Barcelona, Spain*
[b] *Instituto de Catálisis y Petroleoquímica, CSIC, C/Marie Curie s/n, 28049 Cantoblanco, Madrid, Spain*

Received 31 July 2003; revised 20 October 2003; accepted 10 December 2003

Abstract

The effect of sodium promoter on cobalt–zinc oxide catalysts was studied. Catalysts with different sodium contents (up to 1% (w/w)) were prepared by a coprecipitation method. They were studied in the steam reforming of ethanol between 523 and 723 K and characterized by transmission electron microscopy, X-ray diffraction, Raman and infrared spectroscopies, X-ray photoelectron spectroscopy, and in situ diffuse reflectance infrared spectroscopy. A high segregation of sodium on the surface of catalysts took place. The sodium addition had a positive effect on the steam-reforming reaction of ethanol. Under total conversion and in the 623–723 K temperature range, the production of hydrogen from an ethanol–water (C_2H_5OH:H_2O = 1:13 molar) mixture (bioethanol) increased (5–8%) with sodium content. In addition, the incorporation of sodium resulted in the stabilization of the catalysts toward deactivation. In particular, the sodium-promoter effect was related to a decrease in carbon deposition, as evidenced by transmission electron microscopy, Raman spectroscopy, and X-ray photoelectron spectroscopy.

Keywords: Bioethanol; Hydrogen; Cobalt catalyst; Sodium promoter

1. Introduction

H_2 is nowadays considered as an alternative fuel, and its production for use in fuel cells is a subject of current interest [1,2]. To this end, the use of renewable resources derived from biomass is attractive in order to develop sustainable energy systems [3,4]. Ethanol is considered to be an appropriate H_2 reservoir because it can be easily produced from biomass and can be transported safely. Moreover, ethanol has a relatively high hydrogen content, and its reaction with water under steam-reforming conditions is able to produce 6 mol of H_2 per mole of ethanol reacted:

$$CH_3CH_2OH + 3H_2O \rightarrow 6H_2 + 2CO_2.$$

Different catalysts have been studied for the above-noted reaction including oxides [5], nickel- [6,7], nickel–copper- [8,9], noble metals- [10–13], and cobalt-based catalysts [14–17]. However, only a few of these studies included long-term catalytic studies or the characterization of catalysts after catalytic tests. Carbon deposition has been shown to cause deactivation of nickel-, nickel–copper-, and cobalt-based catalysts [6,7,9,15]. For cobalt-based catalysts, this deactivation depended on the support, and increased with reaction temperature [15]. We recently studied ZnO-supported cobalt catalysts which were very effective in the steam-reforming reaction, but showed abundant carbon deposition after reaction [17]. In this paper we describe the preparation of new cobalt–ZnO-based catalysts by a coprecipitation method from nitrate salts and sodium carbonate. The promoter effect of sodium in the enhancement of catalytic performance, mainly the stability and extent of carbon deposition, is analyzed.

2. Experimental methods

2.1. Preparation of catalysts

Catalysts were prepared by the coprecipitation method from $Zn(NO_3)_2$ and $Co(NO_3)_2$ aqueous solutions. Precipita-

* Corresponding author.
E-mail address: pilar.piscina@qi.ub.es (P. Ramírez de la Piscina).

0021-9517/$ – see front matter
doi:10.1016/j.jcat.2003.12.008

tion was accomplished by the addition of a Na_2CO_3 solution at 313 K. After aging at 313 K for 1.5 h, the resulting suspension was filtered and divided into several fractions. Each fraction was washed with distilled water to a different extent in order to obtain materials with different sodium contents. The resulting solids were then dried at 363 K overnight and calcined in air at 673 K for 12 h. Samples were reduced under hydrogen at 673 K for 12 h and labeled as aNaCoZn (a = % wt/wt Na). Chemical analyses performed by optical emission spectroscopy with inductively coupled plasma (ICP-OES) revealed that the cobalt content for all samples was ca. 10% by weight, whereas the sodium content was in the range 0–1% by weight.

2.2. Catalyst characterization

Samples for high-resolution transmission electron microscopy (HRTEM) were deposited on copper grids with a holey-carbon-film support from methanol suspensions. The instrument used was a Philips CM-30 electron microscope equipped with a LaB_6 source and operated at 300 kV, with a 0.19-nm point resolution. Magnification and camera constants were calibrated using appropriate standards under the same electron-optical conditions. For data treatment, Fourier-transformed images were obtained by using local software on digitalized parts of the negatives.

X-ray diffraction profiles (XRD) were collected in the 2θ angle between 10° and 70°, at a step width of 0.02° and by counting 10 s at each step with a Siemens D-500 instrument equipped with a Cu target and a graphite monochromator.

Raman spectra were obtained with a Jobin Yvon T64000 spectrometer using an Ar ion laser as an illumination source (514.5 nm) and a CCD detector cooled at 140 K. The Raman instrument was coupled to a standard Olympus microscope ($\times 50$ magnification) and the collection optics system was used in the backscattering configuration. The laser power at the sample was limited to less than 3 mW in order to avoid laser heating effects. Spectra were recorded in the ranges 280–830 and 1170–1720 cm^{-1}.

Photoelectron spectra (XPS) were acquired with a VG ESCALAB 200R spectrometer equipped with a Mg-K_α ($h\nu = 1253.6$ eV, 1 eV $= 1.6022 \times 10^{-19}$ J) X-ray exciting source, a hemispherical electron analyzer, and a pretreatment chamber. The residual pressure in the ion-pumped analysis chamber was maintained below 4.2×10^{-9} mbar (1 mbar = 101.33 Pa) during data acquisition. The binding energies (BE) were referred to the C 1s peak of adsorbed paraffinic hydrocarbons at 284.9 eV or the Zn $2p_{3/2}$ peak of ZnO at 1022.0 eV, which gave BE values with an accuracy of ±0.1 eV. Peak intensity was calculated as the integral of each peak after smoothing and subtraction of a Shirley background [18] and fitting of the experimental curve to Gaussian/Lorentzian lines.

Infrared spectra (FTIR) were obtained at room temperature on a Nicolet 520 Fourier transform instrument at 2 cm^{-1} of resolution by collecting 100 scans. For these experiments special greaseless vacuum cells with CaF_2 windows which allowed thermal treatments were used.

For in situ infrared experiments, about 20 mg of catalyst was placed in a Spectra Tech catalytic chamber on a Nicolet Magna 750 infrared spectrometer, operating in diffuse reflectance mode (DRIFT). A reactant mixture ethanol/water (1/13 mol/mol) was admitted in the chamber at atmospheric pressure by saturating a helium stream (total flow = 20 ml min^{-1}, 0.4 kPa ethanol). Analogously, an acetaldehyde-saturated stream was obtained by bubbling He at room temperature through pure acetaldehyde (99.5%). The reactor outlet was connected on-line to a QMS200 Baltzers quadrupole mass spectrometer (MS).

2.3. Catalytic test

Catalytic studies of ethanol steam reforming were performed at atmospheric pressure in a U-shaped quartz reactor (5-mm internal diameter). The amount of 100 mg of catalyst was charged and diluted with inactive SiC, giving a catalyst bed volume of 0.6 ml. A constant mixture of EtOH:H_2O = 20:80 by volume (EtOH:$H_2O \sim$ 1:13 molar basis, HPLC purity grade) was supplied by a Gilson 307 piston pump, the mixture being vaporized at 453 K and diluted with Ar (purity 99.9995%) before entering the reaction chamber (($C_2H_5OH + H_2O$):Ar = 1:5 molar basis). GHSV was 5000 h^{-1}.

The temperature of the catalyst was first raised to 523 K under Ar, and then the EtOH + H_2O mixture was added. Catalysts were tested under the following sequence of temperature and time: 523 K (2 h) → 573 K (20 h) → 623 K (2 h) → 673 K (2 h) → 723 K (20 h) → 573 K (2 h) → 523 K (2 h). At the end of the catalytic test the flow of EtOH + H_2O was stopped and the catalyst was cooled under an Ar stream and stored for HRTEM, Raman, and XPS studies. Over the 0.98NaCoZn catalyst, an additional long-term catalytic test was carried out at 673 K for 10 days.

Experiments of acetaldehyde steam reforming (CH_3CHO:H_2O = 1:13, ($CH_3CHO + H_2O$):Ar = 1:5 molar basis) were conducted in a similar way with the same catalytic test device in a temperature range 523–723 K, and 20–30 mg of catalyst diluted with SiC was used (GHSV = 5000 h^{-1}).

The analysis of the reactants and all the reaction products was carried out on-line by gas chromatography as described previously [15]. The detection limit of CO was ca. 20 ppm. Response factors for all products were obtained with appropriate standards before and after each catalytic test.

Selectivity of products was calculated on the basis of molar percentage of each product evolved (water excluded) with respect to the total moles of products formed.

3. Results and discussion

3.1. Characterization of catalysts

The Co–ZnO catalysts with different sodium contents prepared in this study are compiled in Table 1.

X-ray diffraction patterns of samples after the calcination treatment at 673 K contained peaks due to ZnO and Co_3O_4 phases. After reduction, XRD profiles showed, in all cases, the presence of crystalline ZnO and metallic cobalt phases (Fig. 1A). However, an analysis of the zone in which the most intense peak of CoO is located, ($2\theta = 42.6°$, CoO(200)), indicates that the presence of CoO cannot be ruled out (Fig. 1B).

The characterization of 0.98NaCoZn by Raman spectroscopy also pointed to the presence of oxidized cobalt. A strong, broad band at 521 cm^{-1} and a shoulder at 555 cm^{-1} were related to the presence of CoO [19], whereas weak bands appearing at 696 and 477 cm^{-1} may indicate the simultaneous presence of Co_3O_4 [20].

Table 1
Sodium and cobalt content and BET surface areas of catalysts

Catalyst	Wt% Co	Wt% Na	BET (m^2 g^{-1})
0.06NaCoZn	11.1	0.06	16.1
0.23NaCoZn	10.8	0.23	16.1
0.78NaCoZn	10.8	0.78	15.2
0.98NaCoZn	10.5	0.98	15.5

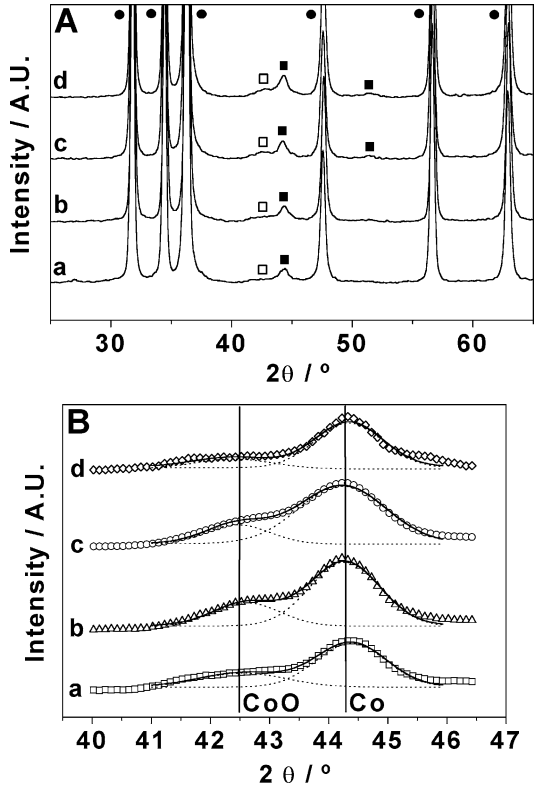

Fig. 1. X-ray diffraction patterns of reduced catalysts before the catalytic test. (A) 2θ range 25–65°, (B) 2θ range 40–46.5°. (a) 0.06NaCoZn; (b) 0.23 NaCoZn; (c) 0.78NaCoZn; (d) 0.98NaCoZn. ■, Co phase; □, CoO phase; ●, ZnO phase.

Table 2
Binding energies (eV) and surface atomic ratios of NaCoZn catalysts before catalytic test

Catalyst	Zn $2p_{3/2}$	Na 1s	Co $2p_{3/2}$[a]	Co/Zn	Na/Zn
0.06NaCoZn	1022.0	1072.4	778.3 (40) 780.5 (60)	0.336	0.076
0.23NaCoZn	1021.9	1072.3	778.3 (37) 780.4 (63)	0.309	0.150
0.78NaCoZn	1021.9	1072.4	778.3 (53) 780.2 (47)	0.323	0.416
0.98NaCoZn	1022.0	1072.5	778.3 (45) 780.1 (55)	0.216	0.314

[a] Values in parentheses are peak area percentages.

The 0.98NaCoZn catalyst was also studied after reduction by TEM-derived techniques (Fig. 2). High-resolution transmission electron microscopy showed lattice spacings in direct space corresponding to ZnO and Co_3O_4 phases. Numerous Moiré fringes were visible in this sample which deserved further study. As a representative example, Fig. 2 shows the Fourier-transformed image of the Moiré pattern delimited by the inset along with reconstructed images corresponding to the different spots. From the analysis in reciprocal space it is deduced that the inset contains a superposition of ZnO, Co_3O_4, and Co phases.

The characterization of 0.06NaCoZn after reduction by TEM-derived techniques showed the presence of metallic cobalt and CoO particles, as well as ZnO (Fig. 3), which agrees with XRD. Insets in Fig. 3 display the Fourier-transformed image of zones A and B in the micrograph, which correspond to Co, CoO, and ZnO phases.

The Zn $2p_{3/2}$, Co $2p_{3/2}$, and Na 1s core level spectra were recorded for all samples. The binding energy values are compiled in Table 2. Two components and a satellite line in the Co $2p_{3/2}$ region were observed for all catalysts. The component at 778.3 eV is assigned to fully reduced cobalt species and the second component at higher binding energies, 780.1–780.5 eV, is associated with high-spin Co^{2+} ions, in accordance with the intense satellite line at higher binding energies [21]. From the integrated peak areas and atomic sensitivity factors [22], the atomic ratios Co/Zn and Na/Zn were calculated (see Table 2). A high segregation of sodium on the surface of the catalysts took place. The Na/Zn atomic ratios determined by XPS are much higher than those determined by ICP-OES and they increased with the sodium content up to 0.78% Na. Fig. 4 depicts the Na/Co surface ratio determined by XPS with respect to the Na/Co ratio corresponding to the bulk composition of the catalysts. An increase of the Na/Co ratio determined by XPS with respect to the bulk Na/Co ratio is evident. This increase was linear up to 0.78NaCoZn catalyst.

Chemisorption of CO at room temperature over reduced catalysts was followed by FTIR. The 0.06NaCoZn catalyst showed bands at 2103 and 2056 cm^{-1}, which were assigned to υ(CO) of $Co(CO)_n$ species [23]. None of the other cat-

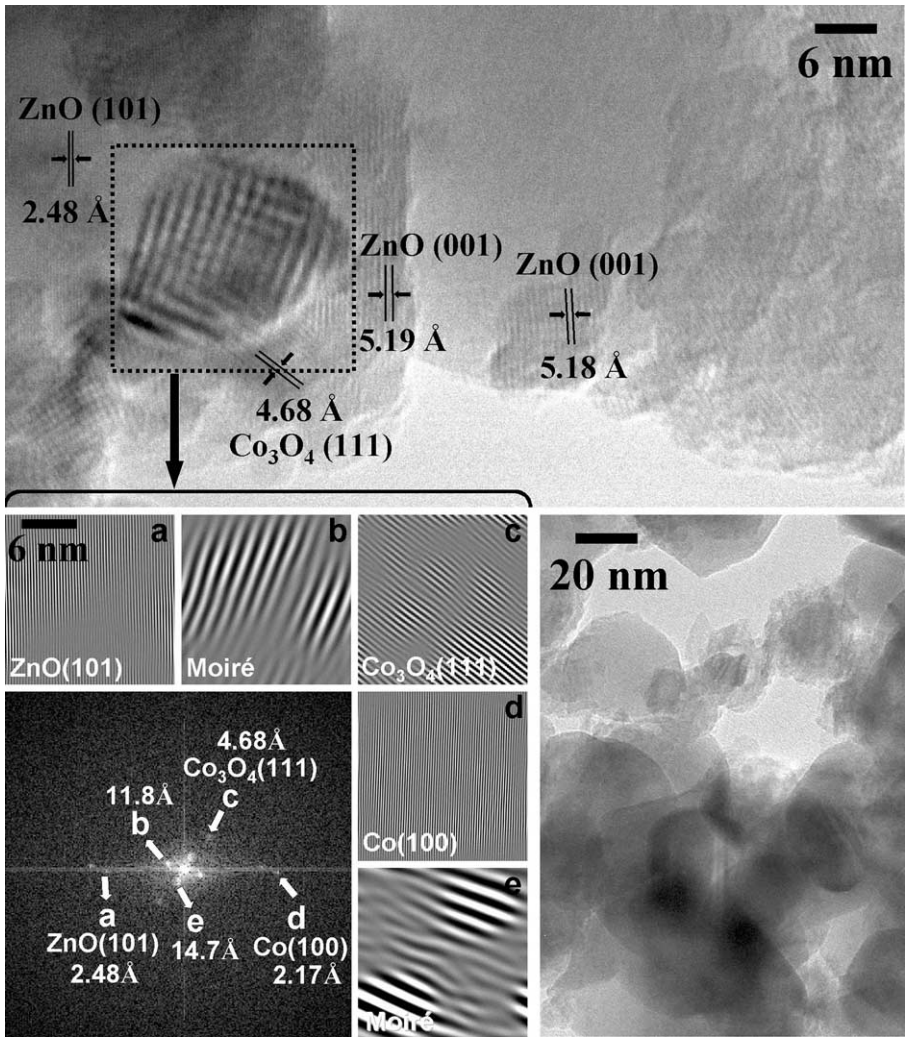

Fig. 2. High-resolution transmission electron microscopy images of 0.98NaCoZn before catalytic test. Fourier-transformed image of the inset and reconstructed images corresponding to the different spots are included.

alysts showed υ(CO) bands; this fact may be related to the higher segregation of sodium on the surface determined by XPS, which may be deposited on the surface of cobalt particles.

Catalysts were characterized after the catalytic tests. HRTEM analysis of the 0.98NaCoZn catalyst again showed numerous Moiré fringes due to the superposition of ZnO and cobalt-containing phases, such as metallic cobalt and CoO. Fig. 5 depicts a lattice fringe image along with Fourier-transformed images of selected areas showing spacings corresponding to ZnO and metallic cobalt, as well as CoO. No carbonaceous deposits were found on this catalyst by this technique after the catalytic test.

However, a TEM study of 0.06NaCoZn after the catalytic test showed Co and CoO particles surrounded by poorly ordered phases (Fig. 6). Fig. 6 also shows a high-resolution image of one of these particles (labeled as A). A 3.8 Å spacing for C(002) characteristic of poorly graphitized carbon is visible. Analysis of zone (a) indicates the segregation of CoO exhibiting (200) planes. The Fourier-transformed images in the insets of zone (a) and (b) contain spots corresponding to CoO(200) planes at 2.13 Å and Co(111) planes at 2.06 Å, respectively.

In order to obtain more information about carbon deposition, Raman spectra in the zone 1200–1700 cm^{-1} and XPS of C 1s level were recorded for samples after catalytic tests.

Raman spectra are given in Fig. 7. Samples 0.06NaCoZn and 0.23NaCoZn showed two bands centered at 1340 and 1590 cm^{-1}, which are characteristic of poorly ordered carbon deposits [24]. Catalysts with higher contents of sodium, 0.78NaCoZn and 0.98NaCoZn, showed no bands in this zone, indicating that carbon quantities are below the Raman microspectrometer detection limit.

The binding energy region of C 1s core-level of two representative samples (0.06NaCoZn and 0.98NaCoZn) is shown in Fig. 8. For the 0.98NaCoZn sample, four photoemission peaks appear at binding energies of 284.3, 284.9, 286.3, and 290.0 eV. These peaks are due to graphitic carbon, adsorbed hydrocarbons, species containing C–O bonds, and surface carbonate species [25,26]. 0.06NaCoZn sam-

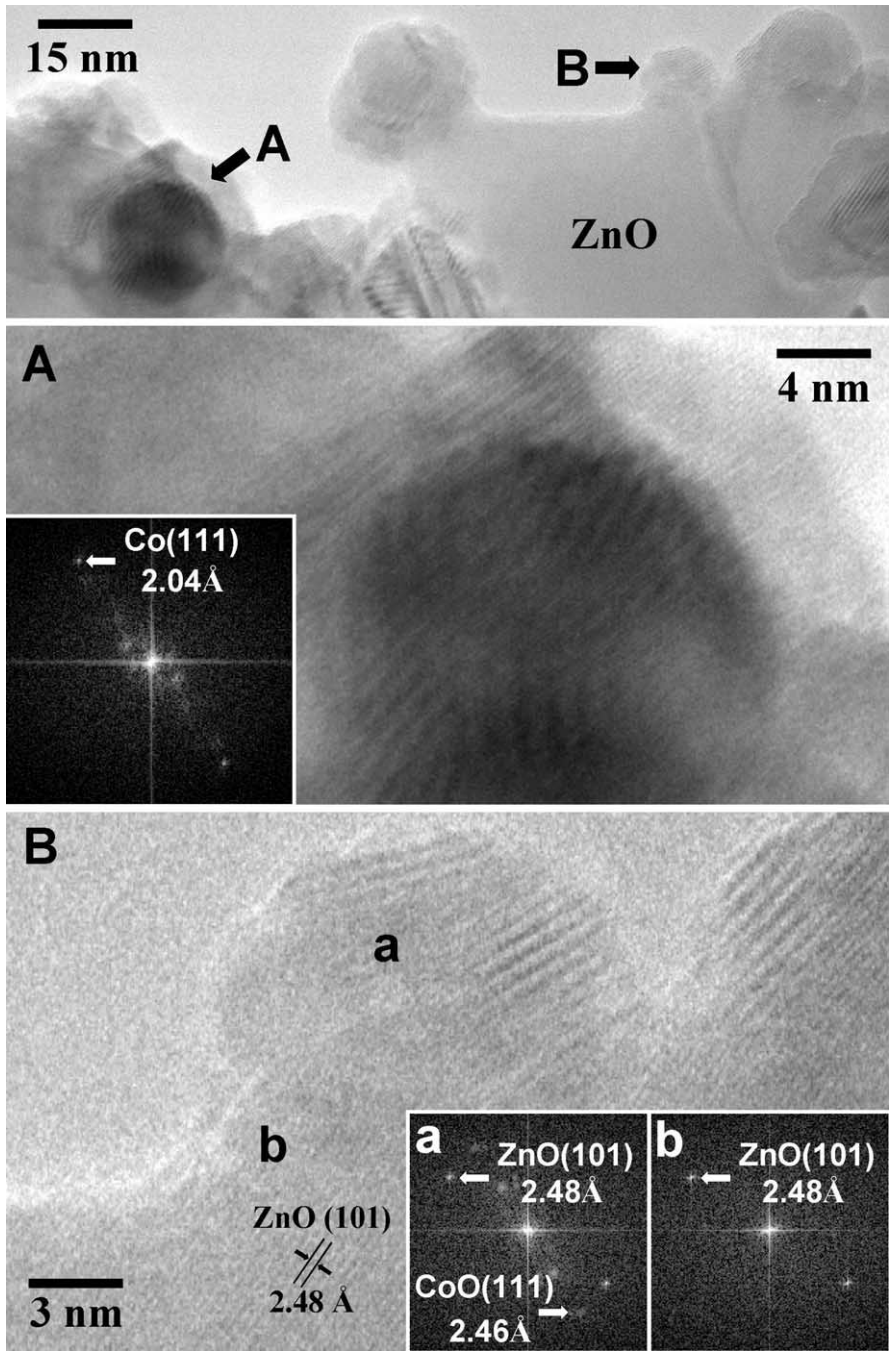

Fig. 3. High-resolution transmission electron microscopy images of 0.06NaCoZn before catalytic test. The insets correspond to Fourier-transformed images of marked areas.

ple exhibits a very intense peak centered a 284.5 eV due to graphitic carbon and a peak toward 289.3 eV due to carboxylate species. Surface carbon determined by XPS is very much higher for 0.06NaCoZn than for 0.98NaCoZn, which is consistent with Raman results.

As regards carbon deposition during the reaction, the behavior of 0.78NaCoZn and 0.98NaCoZn catalysts contrasts with that of other reported ZnO-supported cobalt catalysts which, after similar catalytic tests, have shown carbonaceous deposits; these catalysts contained no sodium and were prepared by impregnation of different precursors [15,17].

To evaluate the catalytic stability of 0.98NaCoZn material, a long-term catalytic test was carried out (240 h at 673 K) and a Raman spectrum was then taken. In neither case did bands appear in the 1700–1200 cm^{-1} zone, indicating again that carbonaceous residues, if present, are below the detection limit of the technique (see spectrum e, Fig. 7).

These characterization results point to a promoter effect of sodium on catalyst stability. The absence of carbon deposits on the catalysts can be related to the sodium presence on the surface.

3.2. Catalytic performance

Tables 3–6 show the catalytic behavior of each sample over time between 523 and 723 K. All catalysts showed a good performance in the ethanol steam-reforming reaction between 623 and 723 K. For all of them, in this temperature range, total ethanol conversion was attained and high yields to H_2 and CO_2 were obtained. In all cases the main reaction which took place, under the experimental conditions used, was ethanol steam reforming. When catalysts operated at low conversion values (< 10%), at 523 K and initial reaction times, only H_2 and acetaldehyde (ca. 1:1 molar basis) were produced due to the dehydrogenation of ethanol. For these catalytic systems this is the first step in the ethanol steam-reforming reaction. The initial activity at 523 K for the dehydrogenation of ethanol decreased with the sodium content of the catalyst, this probably being related to the high sodium segregation on the surface, as determined by XPS. Sodium species may block surface cobalt active sites according with results of CO chemisorption followed by FTIR. However, for higher conversion values at 573 K, when the reforming of acetaldehyde takes place, an increase of sodium content in the catalyst produces a decrease in the residual acetaldehyde (see Tables 3–6).

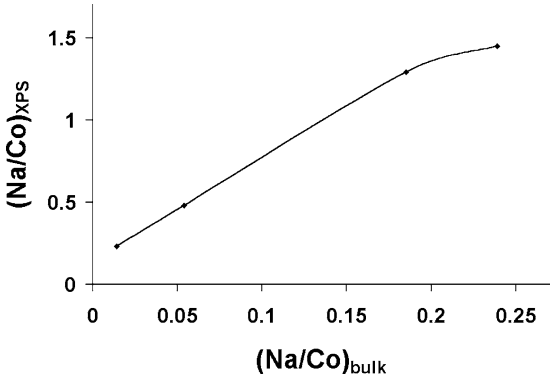

Fig. 4. Na/Co atomic ratio determined by XPS versus the Na/Co bulk ratio determined by ICP-OES for different NaCoZn catalysts.

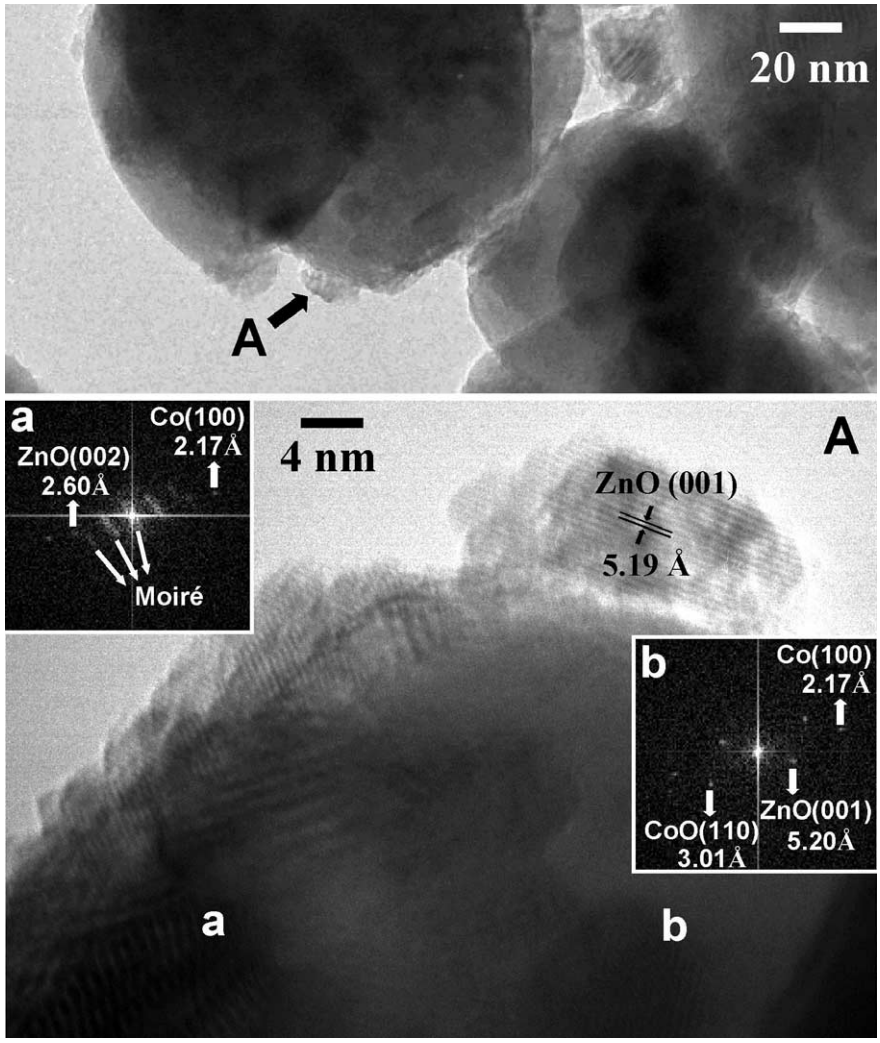

Fig. 5. High-resolution transmission electron microscopy images of 0.98NaCoZn after steam reforming of ethanol at 723 K. The insets correspond to Fourier-transformed images of marked areas.

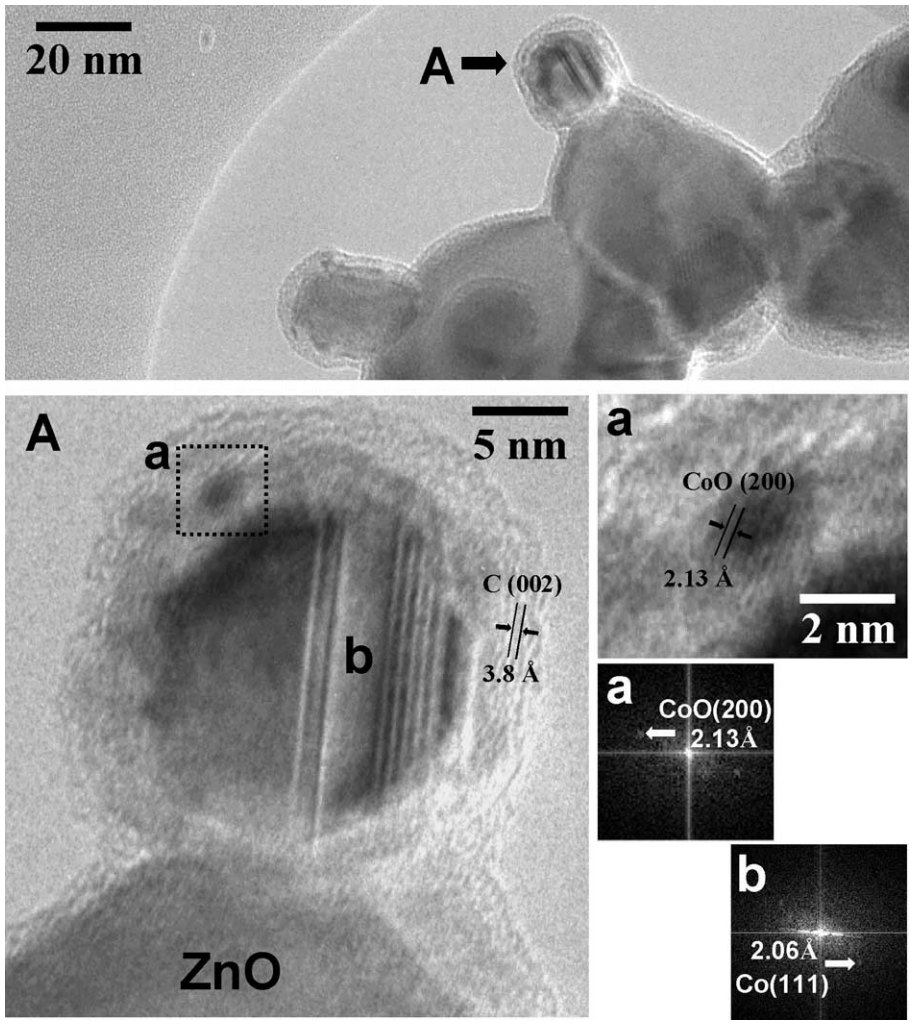

Fig. 6. High-resolution transmission electron microscopy images of 0.06NaCoZn after steam reforming of ethanol at 723 K, and derived Fourier-transformed patterns.

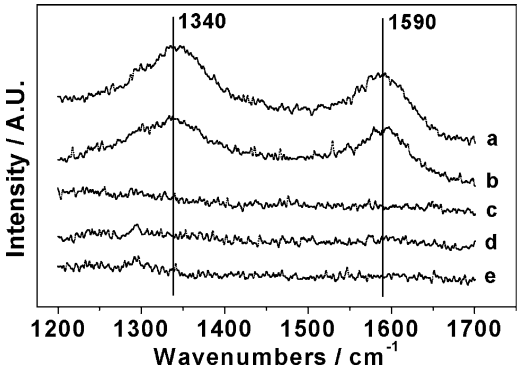

Fig. 7. Raman spectra of catalysts after catalytic tests: (a) 0.06NaCoZn; (b) 0.23NaCoZn; (c) 0.78NaCoZn; (d) 0.98NaCoZn; (e) 0.98NaCoZn catalyst after the long-term catalytic test.

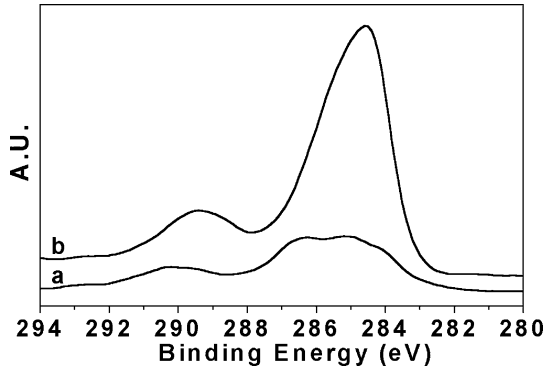

Fig. 8. XP spectra corresponding to C 1s zone: (a) 0.98NaCoZn; (b) 0.06 NaCoZn.

To better understand the overall process, we have carried out the reforming of acetaldehyde under similar experimental conditions. Catalytic tests were performed over 0.06 NaCoZn and 0.78NaCoZn catalysts (Table 7). At low conversion values, both catalysts produced moderate amounts of CO and CH_4 in addition to CO_2 and H_2, but the selectivity depended on the sodium content of the catalyst. The 0.78 NaCoZn catalyst showed higher selectivity to CO and lower selectivity to CH_4 with respect to catalyst 0.06NaCoZn, thus indicating a lower ability for hydrogenation of 0.78NaCoZn. Over 0.78NaCoZn and under high conversion values, high

Table 3
Catalytic behavior of 0.06NaCoZn in the ethanol steam reforming

T (K)	t (h)	Activity (mol C_2H_5OH/ mol Co h)	C_2H_5OH conversion (%)	Selectivity[a] (%)					mol H_2/ mol C_2H_5OH	mol CO_2/ mol C_2H_5OH
				H_2	CO	CO_2	CH_4	CH_3CHO		
523	2	0.38	7	49.8	–	–	–	50.2	0.07	–
573	4	4.18	76.3	70.8	–	22.3	1.4	5.4	3.12	0.98
573	24	4.20	76.6	69.6	–	21.0	1.4	8.0	2.79	0.84
623	26	n.a.	100	72.3	–	25.0	2.7	–	5.22	1.81
673	28	n.a.	100	72.1	0.2	24.9	2.8	–	5.17	1.78
723	30	n.a.	100	72.8	0.3	24.8	2.2	–	5.35	1.82
723	50	n.a.	100	73.1	0.7	24.5	1.6	–	5.44	1.83
573	52	3.31	60.5	64.9	1.4	16.3	2.2	15.2	1.56	0.39
523	54	0.09	1.7	46.2	–	–	4.0	49.8	0.02	–

Reaction conditions: total pressure, 1 atm; EtOH:H_2O:Ar = 1:13:70 (molar ratio); GHSV = 5000 h^{-1}.
[a] Molar percentage of products (water excluded).

Table 4
Catalytic behavior of 0.23NaCoZn in the ethanol steam reforming

T (K)	t (h)	Activity (mol C_2H_5OH/ mol Co h)	C_2H_5OH conversion (%)	Selectivity[a] (%)					mol H_2/ mol C_2H_5OH	mol CO_2/ mol C_2H_5OH
				H_2	CO	CO_2	CH_4	CH_3CHO		
523	2	0.16	2.9	50.5	–	–	–	49.5	0.03	–
573	4	4.03	71.6	72.5	–	23.7	1.2	2.6	3.45	1.13
573	24	4.15	73.7	72.6	–	23.8	1.0	2.5	3.58	1.17
623	26	n.a.	100	73.9	–	25.0	1.1	–	5.66	1.91
673	28	n.a.	100	73.4	–	25.0	1.6	–	5.51	1.88
723	30	n.a.	100	73.6	0.6	24.6	1.2	–	5.58	1.86
723	50	n.a.	100	73.7	0.1	24.9	1.2	–	5.61	1.90
573	52	3.75	66.7	71.0	–	22.3	1.3	5.4	2.76	0.87
523	54	0.37	6.5	50.4	–	–	–	49.6	0.07	–

Reaction conditions: total pressure, 1 atm; EtOH:H_2O:Ar = 1:13:70 (molar ratio); GHSV = 5000 h^{-1}.
[a] Molar percentage of products (water excluded).

Table 5
Catalytic behavior of 0.78NaCoZn in the ethanol steam reforming

T (K)	t (h)	Activity (mol C_2H_5OH/ mol Co h)	C_2H_5OH conversion (%)	Selectivity[a] (%)					mol H_2/ mol C_2H_5OH	mol CO_2/ mol C_2H_5OH
				H_2	CO	CO_2	CH_4	CH_3CHO		
523	2	0.08	1.4	50.4	–	–	–	49.6	0.01	–
573	4	3.73	66.3	73.0	–	24.4	1.2	1.5	3.39	1.13
573	24	3.74	66.5	73.1	–	24.2	1.1	1.6	3.41	1.13
623	26	n.a.	100	73.8	–	25.0	1.2	–	5.63	1.91
673	28	n.a.	100	74.2	–	25.0	0.9	–	5.75	1.93
723	30	n.a.	100	73.9	0.5	24.6	1.0	–	5.65	1.89
723	50	n.a.	100	74.0	–	25.0	1.0	–	5.69	1.92
573	52	3.66	65.1	73.3	–	24.3	0.9	1.4	3.39	1.13
523	54	0.37	6.6	54.3	–	4.5	0.1	41.1	0.08	0.01

Reaction conditions: total pressure, 1 atm; EtOH:H_2O:Ar = 1:13:70 (molar ratio); GHSV = 5000 h^{-1}.
[a] Molar percentage of products (water excluded).

selectivity to CO_2 and H_2 were achieved (near the stoichiometric values for the steam-reforming reaction), and only minor amounts of CO and CH_4 were obtained, as was the case for the ethanol steam reforming (see Table 5).

In situ DRIFT experiments under reaction conditions were carried out, and the products evolved were analyzed by MS. At 573 K, 0.06NaCoZn shows bands at 1620, 1585, and 1430 cm^{-1} (Fig. 9A, spectrum a). The band at 1620 cm^{-1} is assigned to the bending mode of molecular water. The other two bands can be reasonably assigned to υ_{assym}OCO and υ_{sym}OCO of bridged or bidentate acetate species [27, 28]. These bands increased when the reaction was quenched under helium (Fig. 9A, spectra b and c). Given that acetaldehyde is an intermediate species in the reforming reaction,

Table 6
Catalytic behavior of 0.98NaCoZn in the ethanol steam reforming

T (K)	t (h)	Activity (mol C_2H_5OH/ mol Co h)	C_2H_5OH conversion (%)	Selectivity[a] (%)					mol H_2/ mol C_2H_5OH	mol CO_2/ mol C_2H_5OH
				H_2	CO	CO_2	CH_4	CH_3CHO		
523	2	0.06	1.1	49.4	–	––	–	50.6	0.01	–
573	4	3.59	62.2	73.3	–	24	1.7	1.0	3.48	1.14
573	24	3.68	63.8	73.4	–	24.5	1.0	1.1	3.23	1.08
623	26	n.a.	100	73.3	0.4	24.6	1.7	–	5.48	1.84
673	28	n.a.	100	73.3	–	25	1.6	–	5.50	1.88
723	30	n.a.	100	74.4	–	24.9	0.7	–	5.80	1.94
723	50	n.a.	100	74.2	–	24.9	0.9	–	5.76	1.93
573	52	3.60	62.4	73.8	–	24.5	0.7	1.1	3.37	1.12
523	54	0.36	6.3	52.8	–	3.3	0.6	43.3	0.07	0.01

Reaction conditions: total pressure, 1 atm; $EtOH:H_2O:Ar = 1:13:70$ (molar ratio); GHSV = 5000 h^{-1}.
[a] Molar percentage of products (water excluded).

Table 7
Catalytic behavior of catalysts in the acetaldehyde steam reforming

Catalyst	T (K)	t (h)	Activity (mol CH_3CHO/ mol Co h)	CH_3CHO conversion (%)	Selectivity[a] (%)				mol H_2/ mol CH_3CHO	mol CO_2/ mol CH_3CHO
					H_2	CO	CO_2	CH_4		
0.06NaCoZn	573	4	3.9	14.3	68.1	2.9	26.4	2.6	0.61	0.24
0.78NaCoZn	573	4	3.04	13.5	68.6	5.4	25.1	0.9	0.59	0.22
	723	30	21.7	96.4	70.8	0.1	28.4	0.7	4.69	1.88

Reaction conditions: total pressure, 1 atm; $CH_3CHO:H_2O:Ar = 1:13:70$ (molar ratio); GHSV = 5000 h^{-1}.
[a] Molar percentage of products (water excluded).

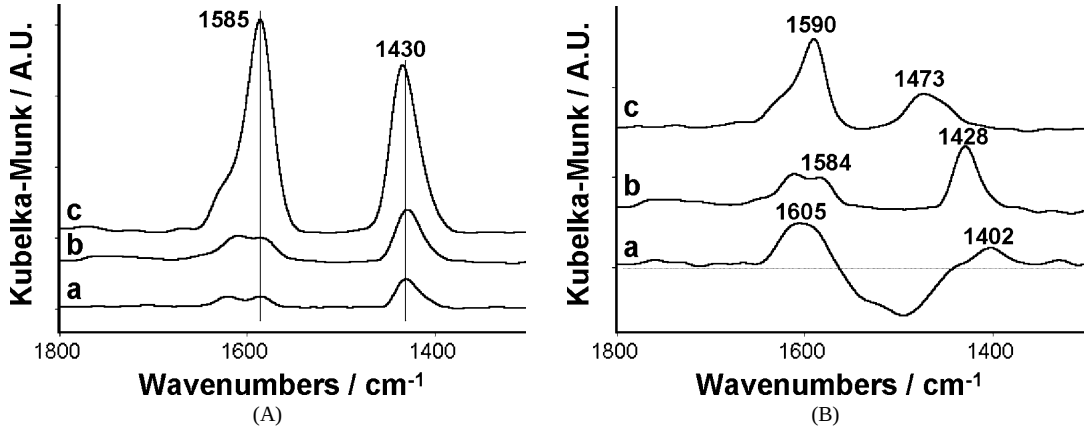

Fig. 9. Diffuse reflectance infrared spectra recorded in situ for (A) 0.06NaCoZn and (B) 0.98NaCoZn. (a) Under reaction conditions at 573 K; (b) after a, reaction mixture was cut off and helium was introduced at 573 K; (c) after b, temperature was decreased till 298 K.

its chemisorption was followed by DRIFT in separate experiments. Analogous bands at 1589 and 1428 cm^{-1} related to acetate species appeared after interaction of acetaldehyde with 0.06NaCoZn (Fig. 10, spectrum a), which remained after flushing with helium to at least 473 K. Fig. 9B shows the spectra obtained under reaction conditions at 573 K for the 0.98NaCoZn catalyst (spectrum a). A negative broad absorption (1450–1550 cm^{-1}) due to the disappearance of carbonate species present in the initial catalyst is visible. Carbonate species were recovered when the catalyst was flushed with helium (Fig. 9B, spectra b and c). Spectra b and c in Fig. 9B show bands which could be assigned to the presence of acetate species. However, under reaction conditions, the spectrum of this catalyst differs from that of 0.06NaCoZn. Small and broad bands centered at 1605 and 1402 cm^{-1} appeared. These bands may be assigned to formate species [29], although the simultaneous presence of acetate species cannot be ruled out. The 0.98NaCoZn catalyst exposed to acetaldehyde and then flushed with helium at 473 K shows again the disappearance of carbonate species (Fig. 10, spectrum b). The spectrum is rather complex, and the observed bands cannot be unambiguously ascribed to individual species. Ethoxy and acetate species seems to be present, but the presence

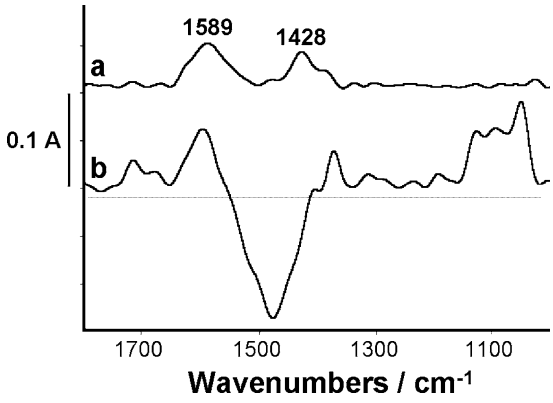

Fig. 10. Diffuse reflectance infrared spectra after acetaldehyde chemisorption on catalysts. Acetaldehyde was chemisorbed on catalysts at room temperature and then they were flushed with helium at 473 K. (a) 0.06NaCoZn and (b) 0.98NaCoZn.

of formate and other surface species cannot be discarded [28,30].

These experiments show that the interaction of acetaldehyde with catalysts depends on their sodium content. Their catalytic behavior could be affected by this different interaction.

From DRIFT and catalytic results we propose that the steam reforming of ethanol over Co/ZnO systems involves in a first step the dehydrogenation of ethanol to acetaldehyde. Then, acetaldehyde is reformed via acetate species. These species have been proposed as intermediates in the acetic acid steam reforming [31].

Other differences in the catalytic performance of catalysts can be established according to their sodium content. A comparison of activity data at 573 K after 24 or 52 h indicates a decrease of deactivation with the increase of sodium content. A 21% deactivation is observed for 0.06NaCoZn and ca. 10% for 0.23NaCoZn, whereas only around 2% deactivation is observed for 0.78NaCoZn and 0.98NaCoZn catalysts. Only the sample with the lowest sodium content, 0.06NaCoZn, showed a deactivation when activity data at 523 K after 2 or 54 h were compared.

As stated above, characterization of postreaction catalysts showed abundant carbon deposition on the low sodium content samples, 0.06NaCoZn and 0.23NaCoZn, which may be related with the deactivation process of these catalysts.

On the other hand, in the acetic acid steam reforming, CH_x species coming from the breaking of C–C bond have been proposed as precursors of carbon deposition [31]. From our experimental results, the role of sodium is clearly related to the depression of carbonaceous deposits, so it will play a role in the evolution of CH_x species under reforming conditions. It is well known that sodium is a promoter in methane steam reforming. For nickel catalysts, it has been recently shown that potassium reduces graphite formation by blocking step sites [32]. Besides that, alkaline additives facilitate the gasification of carbonaceous residues [33].

Over the 0.98NaCoZn catalyst, which showed the best catalytic performance and the highest stability, a long-term catalytic test was carried out at 673 K. No significant changes in the catalytic performance of the catalyst over time (240 h) were found. Under total ethanol conversion, only CH_4 and CO were obtained as by-products; the selectivity to CH_4 was always ca. 1% and that to CO was less than 0.6%.

4. Conclusions

Over Co/ZnO catalysts and under the experimental conditions tested, the steam reforming of ethanol proceeds via dehydrogenation of ethanol to acetaldehyde and further reforming of acetaldehyde through surface acetate species.

A promoter effect of sodium addition to cobalt-based catalysts has been demonstrated. A significant enhancement of catalytic performance in terms of H_2 yield and stability is found when catalysts are compared to unpromoted materials. The suppression of catalyst deactivation is related to the inhibition of carbon deposition.

Acknowledgments

We thank MCYT (MAT 2002-01739) and CIRIT (2001 SGR-00052) for financial support. J.Ll. is grateful to MCYT for a Ramon y Cajal research program and DURSI (Generalitat de Catalunya).

References

[1] J. Rostrup-Nielsen, Phys. Chem. Chem. Phys. 3 (2001) 283.
[2] R.R. Davda, J.W. Shabaker, G.W. Huber, R.D. Cortright, J.A. Dumesic, Appl. Catal. B 43 (2003) 13.
[3] R.D. Cortright, R.R. Davda, J.A. Dumesic, Nature 418 (2002) 964.
[4] M. Asadullah, S. Ito, K. Kunimori, M. Yamada, K. Tomishige, J. Catal. 208 (2002) 255.
[5] J. Llorca, P. Ramírez de la Piscina, J. Sales, N. Homs, Chem. Commun. (2001) 641.
[6] A.N. Fatsikostas, D.I. Kondarides, X.E. Verykios, Catal. Today 75 (2002) 145.
[7] S. Freni, S. Cavallaro, N. Mondello, L. Spadaro, F. Frusteri, Catal. Commun. 4 (2003) 259.
[8] F. Mariño, G. Baronetti, M. Jobbagy, M. Laborde, Appl. Catal. A 238 (2003) 41.
[9] V. Klouz, V. Fierro, P. Denton, H. Katz, J.P. Lisse, S. Bouvot-Mauduit, C. Mirodatos, J. Power Sources 105 (2002) 26.
[10] J.P. Breen, R. Burch, H.M. Coleman, Appl. Catal. B 39 (2002) 65.
[11] V.V. Galvita, G.L. Semin, V.D. Belyaev, V.A. Semikolenov, P. Tsiakaras, V.A. Sobyanin, Appl. Catal. A 220 (2001) 123.
[12] F. Auprêtre, C. Descorme, D. Duprez, Catal. Commun. 3 (2002) 267.
[13] D.K. Liguras, I. Condarides, X.E. Verykios, Appl. Catal. B 43 (2003) 345.
[14] F. Haga, T. Nakajima, H. Miya, S. Mishima, Catal. Lett. 48 (1997) 223.
[15] J. Llorca, N. Homs, J. Sales, P. Ramírez de la Piscina, J. Catal. 209 (2002) 306.
[16] J. Llorca, J.A. Dalmon, P. Ramírez de la Piscina, N. Homs, Appl. Catal. A 243 (2003) 261.

[17] J. Llorca, P. Ramírez de la Piscina, J.A. Dalmon, J. Sales, N. Homs, Appl. Catal. B 43 (2003) 355.
[18] D.A. Shirley, Phys. Rev. B 5 (1972) 4709.
[19] C.A. Melendres, S. Xu, J. Electrochem. Soc. (1984) 2239.
[20] V.G. Hadjiev, M.N. Iliev, I.V. Vergilov, J. Phys. C: Solid State Phys. 21 (1988) L199.
[21] D.C. Frost, C.A. McDowell, I.S. Woolsey, Mol. Phys. 27 (1974) 1473.
[22] C.D. Wagner, L.E. Davis, M.V. Zeller, J.A. Taylor, R.H. Raymond, L.H. Gale, Surf. Interf. Anal. 3 (1981) 211.
[23] N. Sheppard, T.T. Nguyen, in: R.J. Clark, R.E. Hester (Eds.), Advances in Infrared and Raman Spectroscopy, Heyden, London, 1978, p. 67.
[24] P. Lespade, A. Marchand, M. Couzi, F. Cruege, Carbon 22 (1984) 375.
[25] N.M. Rodriguez, P.E. Anderson, A. Wootsch, U. Wild, R. Schlögl, Z. Paál, J. Catal. 197 (2001) 365.
[26] D. Briggs, M.P. Seah (Eds.), Practical Surface Analysis: Auger and X-Ray Photoelectron Spectroscopy, Wiley, Chichester, 1990.
[27] H. Arakawa, T. Fukushima, M. Ichikawa, K. Takeuchi, T. Matsuzaki, Y. Sugi, Chem. Lett. (1985) 23.
[28] A. Yee, S.J. Morrison, H. Idriss, J. Catal. 186 (1999) 279.
[29] G.J. Millar, C.H. Rochester, K.C. Waugh, J. Chem. Soc., Faraday Trans. 88 (1992) 1033.
[30] H. Idriss, C. Diagne, J.P. Hindermann, A. Kiennemann, M.A. Barteau, J. Catal. 155 (1995) 219.
[31] D. Wang, D. Montané, E. Chornet, Appl. Catal. A 143 (1996) 245.
[32] H.S. Bengaard, J.K. Norskov, J. Sehested, B.S. Clausen, L.P. Nielsen, A.M. Molenbroek, J.R. Rostrup-Nielsen, J. Catal. 209 (2002) 365.
[33] S.G. Chen, R.T. Yang, J. Catal. 138 (1992) 12.